*Progress In Electromagnetics Research, PIER 56, 33–51, 2006*

# ANALYSIS OF TRANSMISSION OF A SIGNAL THROUGH A COMPLEX CYLINDRICAL/COAXIAL CAVITY BY TRANSMISSION LINE METHODS

**C. L. Bopp, III and C. M. Butler**

Holcombe Department of Electrical and Computer Engineering
336 Fluor Daniel EIB, Clemson University
Clemson, SC 29634-0915, USA

**Abstract**—The transmission of time-harmonic and transient signals through a complex cylindrical cavity is investigated by methods akin to microwave circuit techniques. The cavity may consist of multiple overlapping cascaded coaxial and circular cylindrical sections whose walls are perfect electric conductors. The sections may have different axial and radial dimensions and may be filled with material having different magnetic and electric properties. The first and last sections of the cavity are coaxial regions where only TEM modes exist, which allows measurements to be performed with proper excitation and termination. The cavity sections may support both a TEM mode and additional higher order modes or may support one or the other. If two sections have a common junction and each supports only one mode, then the junction is modeled by a simple two-port network. When additional modes are present, they are modeled by addition ports at the network junction. Corresponding equivalent transmission lines are associated with each mode at a physical junction. At each junction, scattering parameters are calculated and used to model the interaction of the various modes that exist. The $S$-parameters at each junction are determined separately by solving a simple integral equation that accounts for the structure of the junction and adjoining sections of coaxial and/or cylindrical guide. The cavity fields are, thus, associated with equivalent currents and voltages on transmission lines. A transmission line network is developed from which the input fields, fields at the cavity termination, and junction fields can be found by microwave circuit techniques or by the BLT transmission line analysis. The results from the transmission line method are compared with results calculated from a coupled integral equation analysis which has been carefully validated experimentally and with measured values on laboratory models.

## 1. INTRODUCTION

Cavity problems have piqued the interest of many since the early days of electromagnetic wave propagation study. Solutions and solution techniques to solve many different cavity problems have been developed. In particular, cavities containing cascaded and overlapping cylindrical and coaxial sections have been solved by integral equation techniques [2, 13]. The objective of this paper is to use transmission line techniques to analyze transmission of a signal through a complex cylindrical/coaxial cavity. Utilizing transmission line theory, one can analyze the propagation and coupling of electric and magnetic fields in a cavity structure. The electric and magnetic fields in a cavity are represented as equivalent voltages and currents on transmission lines and cavity apertures are represented by junctions with corresponding scattering parameter matrices. This technique allows for the development of a library of scattering parameter matrices for isolated junctions which can be called upon to facilitate very efficient determination of fields in complex cavities comprising various configurations of the junctions and sections whose properties are available from the library.

Electric and magnetic fields in waveguides can be defined as quantities analogous to voltages and currents on transmission lines as shown by Montgomery, Dicke, and Purcell in [12] and by Kerns in [7]. They demonstrate that, if the normalizations are chosen such that the complex power flow on the transmission line is equal to that in a guide, then the waveguide can be represented as a microwave circuit of equivalent transmission lines. Kerns extends the method to create a discrete mode model of the coupling of two antennas [8].

Haskal [5] expanded the normalization method of Montgomery et al. and Kerns to include evanescent modes, which are needed to accurately model waveguides when discontinuities are in close proximity. A generalized scattering matrix approach for solving waveguide problems is found in [3, 11]. Ling [10] determines the radar cross section of a cavity with uniform waveguide sections connected by arbitrary discontinuity regions with a method that characterizes each discontinuity by a scattering matrix. In addition to waveguide problems, scattering matrices and equivalent microwave circuits have been used to analyze scattering from antennas and to analyze multi-layered periodic structures. Examples are found in the work of Kahn [6], Lee [9], and Hall, Mittra, and Mitzner [4].

The objective of this paper is to provide an alternate highly-efficient and versatile approach for solving cavity problems. In particular, cavities consisting of multiple cascaded or overlapping

circular-cylindrical and coaxial sections are examined. A technique for computing these fields by transmission line methods is presented. The dimensions of a given cavity section are fixed but from one section to another the dimensions may vary both in the radial and axial directions. The electric and magnetic fields in the cavity are represented as equivalent voltages and currents on a transmission line via a normalization technique that conserves complex power, and cavity apertures are represented as transmission line junctions with equivalent scattering parameter matrices. A transmission line matrix equation for the voltages and currents at transmission line junctions is developed and solved numerically by means of the BLT method [1]. Results from the transmission line model method are compared with integral equation solutions, whose accuracy has been previously verified in [2, 13], and with measured values. The transmission line model data compare favorably with the integral equation and measured results.

## 2. OVERVIEW OF TRANSMISSION LINE MODEL

In the transmission line model, cavity apertures are represented as junctions. These junctions are connected by equivalent transmission lines which represent a cavity section. In Figure 1, a cavity aperture with adjacent coaxial guide sections is shown along with its transmission line model representation. The transmission line model representation for a circular-cylindrical section is the same as that for a coaxial section but with different propagation constants. The fields in a cavity section are represented as equivalent voltages and currents on equivalent transmission lines. Depending on the cavity geometry and excitation, higher order modes may be excited at a particular aperture and may propagate through a guide section. The effect of these higher order modes also must be included in the transmission line model. Additional equivalent transmission lines are added at the junction to account for the higher order modes that are present at the aperture (Figures 1–2) and might couple the field of one aperture to that of another. In general, cutoff higher order modes are not modeled except in cases when two apertures are very close, in which case, the mode or modes must be included.

Coupling between the voltages and currents on different transmission lines occurs only at transmission line junctions (cavity apertures) and is governed by scattering parameters. A scattering parameter matrix is calculated for each junction. For the junctions shown in Figure 1b and Figure 1c, the scattering parameter matrices are of the forms

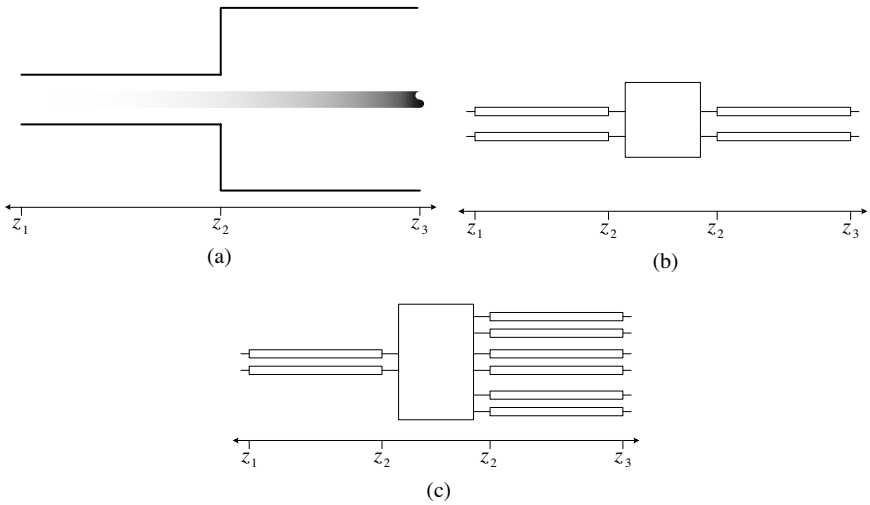


**Figure 1.** Simple cavity aperture (or junction) joining two coaxial cavity sections (shown in (a)) and representation of the cavity junction with equivalent transmission line model for TEM modes only at the aperture (shown in (b)) and for TEM modes in both sections and two higher order modes in the section $z_2 < z < z_3$ (shown in (c)).

$$\left[S^J\right] = \begin{bmatrix} S_{11} & S_{12} \\ S_{21} & S_{22} \end{bmatrix} \tag{1}$$

and

$$\left[S^J\right] = \begin{bmatrix} S_{11} & S_{12} & S_{13} & S_{14} \\ S_{21} & S_{22} & S_{23} & S_{24} \\ S_{31} & S_{32} & S_{33} & S_{34} \\ S_{41} & S_{42} & S_{43} & S_{44} \end{bmatrix}, \tag{2}$$

respectively. The scattering parameters are calculated from a solution of simple integral equations (See Appendix) [2, 13].

Physical voltages and currents in a cavity cannot be explicitly associated with higher order modes. Because the electric field is no longer transverse to the direction of propagation, a potential difference cannot be explicitly determined from the mode electric field. A normalization scheme based on conservation of complex power is used [5, 8]. The transverse electric and magnetic field of a mode (denoted by subscript) in a cavity section may be represented as

$$\boldsymbol{E}_n \cdot \hat{\boldsymbol{\rho}} = E_{n\rho}(\rho, z) = A_{n+} e_{np} e^{-jk_n z} + A_{n-} e_{n\rho} e^{jk_n z} \tag{3}$$

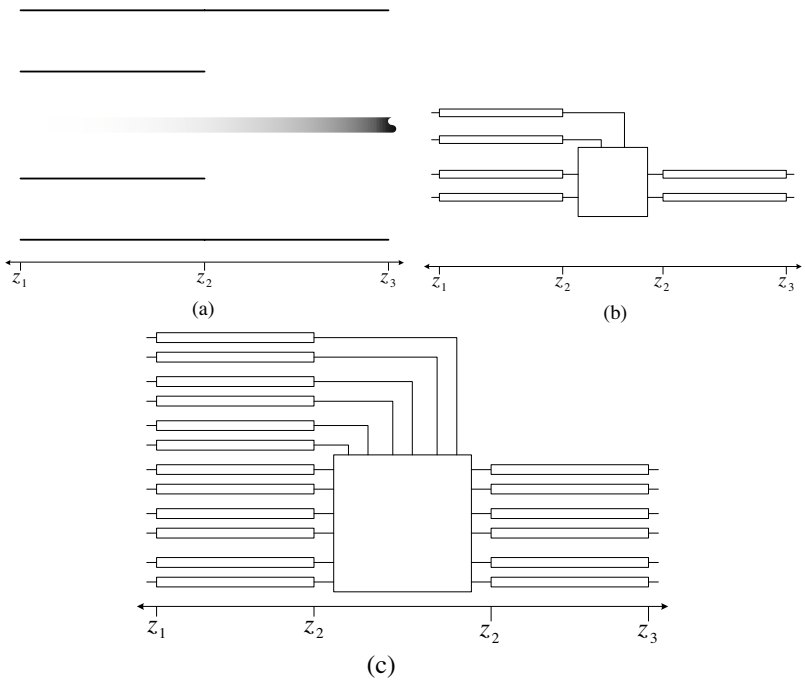


**Figure 2.** Representation of a cavity aperture (or junction) joining three coaxial sections (shown in (a)) and an equivalent transmission line model for TEM modes only at the junction (shown in (b)) and for TEM modes and two higher order modes at the aperture (shown in (c)).

and

$$\boldsymbol{H}_m \cdot \hat{\boldsymbol{\phi}} = H_{m\phi}(\rho, z) = A_{m+} h_{m\phi} e^{-jk_m z} - A_{m-} h_{m\phi} e^{jk_m z}, \tag{4}$$

where $e_{n\rho}$ and $h_{m\phi}$ are normal mode functions and are related by $h_{m\phi} = Y_m^* e_{n\rho}$. Conservation of complex power flow is enforced. In terms of (3) and (4), the complex power in a cavity section is

$$\frac{1}{2} \iint\limits_{\Sigma} \left( \boldsymbol{E}_n^+ \times \boldsymbol{H}_m^{+\,*} \right) \cdot \hat{\boldsymbol{z}} ds = \frac{1}{2} |A_{n+}|^2 \iint\limits_{\Sigma} e_{n\rho} h_{n\phi}^* ds \tag{5}$$

for the modes traveling in the positive $z$ direction and

$$\frac{1}{2} \iint\limits_{\Sigma} \left( \boldsymbol{E}_n^- \times \boldsymbol{H}_m^{-\,*} \right) \cdot \hat{\boldsymbol{z}} ds = -\frac{1}{2} |A_{n-}|^2 \iint\limits_{\Sigma} e_{n\rho} h_{n\phi}^* \, ds \tag{6}$$

for the negative $z$ traveling modes. The equivalent relation

$$\iint\limits_{\Sigma} e_{n\rho} h^*_{m\phi} ds = Y^*_m \iint\limits_{\Sigma} e_{n\rho} e^*_{m\rho} ds = Y^*_m C_n \delta_{nm} \tag{7}$$

is a consequence of the orthogonality of the modes. Letting $C_n = \iint\limits_{\Sigma} e_{n\rho} e^*_{n\rho} ds$, with $C_n$ arbitrary, reduces the above expressions in (5) and (6) to

$$\frac{1}{2} \iint\limits_{\Sigma} \left( \boldsymbol{E}^+_n \times \boldsymbol{H}^{+\,*}_m \right) \cdot \hat{\boldsymbol{z}} ds = \frac{1}{2} |A_{n+}|^2 Y^*_n C_n \tag{8}$$

for the modes traveling in the positive direction and

$$\frac{1}{2} \iint\limits_{\Sigma} \left( \boldsymbol{E}^-_n \times \boldsymbol{H}^{-\,*}_m \right) \cdot \hat{\boldsymbol{z}} ds = -\frac{1}{2} |A_{n-}|^2 Y^*_n C_n \tag{9}$$

for the negative traveling modes. $\Sigma$ is the cross-section area while $A_{n+}$ and $A_{n-}$ are defined in (3) and (4).

The equivalent voltages and currents for a given transmission line mode are represented as

$$v_n = V_{n+} e^{-\gamma_n z} + V_{n-} e^{\gamma_n z} = A A_{n+} e^{-\gamma_n z} + A A_{n-} e^{\gamma_n z} \tag{10}$$

and

$$i_n = I_{n+} e^{-\gamma_n z} + I_{n-} e^{\gamma_n z} = B A_{n+} e^{-\gamma_n z} - B A_{n-} e^{\gamma_n z}, \tag{11}$$

where $A$ and $B$ are undetermined coefficients. The characteristic impedance of the transmission line in our transmission line model is arbitrary. For simplicity, it is chosen to be 1, fixing the relationship $\frac{A}{B} = 1$. The complex power of a given transmission line mode is

$$\frac{1}{2} V_{n+} I^*_{n+} = \frac{1}{2} A B^* |A_{n+}|^2 \tag{12}$$

for the positive traveling waves, and

$$\frac{1}{2} V_{n-} I^*_{n-} = -\frac{1}{2} A B^* |A_{n-}|^2 \tag{13}$$

for the negative. To conserve complex power, the power "carried" by a transmission line must equal that carried by the corresponding cavity mode. Equating the complex power in the cavity with that for the

equivalent transmission lines as given in (12) and (13), one obtains the relationships

$$\frac{1}{2}AB^*|A_{n+}|^2 = \frac{1}{2}|A_{n+}|^2 Y_n^* C_n = \frac{1}{2}|A_{n+}|^2 \tag{14}$$

and

$$-\frac{1}{2}AB^*|A_{n-}|^2 = -\frac{1}{2}|A_{n-}|^2 Y_n^* C_n = -\frac{1}{2}|A_{n-}|^2 \tag{15}$$

where $C_n$ is chosen to be $C_n = \frac{1}{Y_n^*}$. From (14) and (15) and the choice for transmission line impedance, the coefficients $A$ and $B$ are both determined to be of magnitude 1. From the telegraphers equations for a source free region, $\frac{dv_n}{dz} = jk_n C_n i_n$ and $\frac{di_n}{dz} = j\frac{k_n}{C_n} v_n$ where $k_n$ is the propagation constant of the given cavity mode, and the propagation constant $\gamma_n$ for the transmission line model is ascertained to be

$$\gamma_n = \sqrt{(-jk_n C_n I_n)\left(-j\frac{k_n}{C_n}\right)} = jk_n. \tag{16}$$

The $S$-parameter matrices are determined subject to the above constraints and normalizations (See Appendix).

The transmission line model of a complex cavity is created by assembling the individual junctions with associated transmission lines into a transmission line network. An example cavity and its corresponding transmission line network model are shown in Figure 3. The voltages and currents at transmission line junctions are found by the BLT method [1], which is outlined here. The outward going voltages and currents of one junction become the inward going voltages and currents of the connecting or adjacent junction. For the cavity in Figure 3, if we let $V_{\alpha,\beta}^{\gamma}$ denote a line voltage, where $\gamma = ref/inc$ is the reflected/incident voltage on transmission line segment $\alpha$ at junction $\beta$, then the reflected voltages can be related to the incident voltages

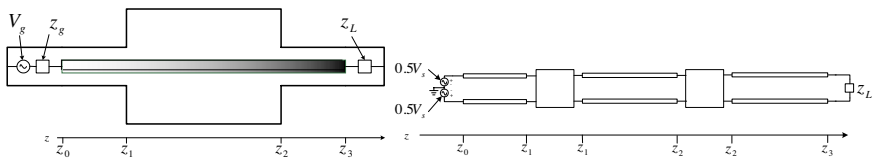


**Figure 3.** A simple two aperture cavity and its corresponding transmission line model representation with only TEM modes modeled.

by

$$\begin{bmatrix} V_{1,S}^{ref} \\ V_{1,1}^{ref} \\ V_{2,1}^{ref} \\ V_{2,2}^{ref} \\ V_{3,2}^{ref} \\ V_{3,L}^{ref} \end{bmatrix} = \begin{bmatrix} 0 & e^{\gamma L_1} & 0 & 0 & 0 & 0 \\ e^{\gamma L_1} & 0 & 0 & 0 & 0 & 0 \\ 0 & 0 & 0 & e^{\gamma L_2} & 0 & 0 \\ 0 & 0 & e^{\gamma L_2} & 0 & 0 & 0 \\ 0 & 0 & 0 & 0 & 0 & e^{\gamma L_3} \\ 0 & 0 & 0 & 0 & e^{\gamma L_3} & 0 \end{bmatrix} \begin{bmatrix} V_{1,S}^{inc} \\ V_{1,1}^{inc} \\ V_{2,1}^{inc} \\ V_{2,2}^{inc} \\ V_{3,2}^{inc} \\ V_{3,L}^{inc} \end{bmatrix} - \begin{bmatrix} \frac{1}{2}V_s \\ -\frac{1}{2}V_s e^{\gamma L_1} \\ 0 \\ 0 \\ 0 \\ 0 \end{bmatrix}, \tag{17}$$

or

$$\left[V^{ref}\right] = [P] \cdot \left[V^{ref}\right] - [V_s], \tag{18}$$

in which the matrix $[P]$ and column vector $[V_s]$ are readily identifiable from (17). The column vector $[V_s]$ is a source vector of traveling voltages where the total differential voltage of the voltage source at $z = 0$ is given by $V_s$. For the particular case shown in Figure 3, the value of the voltage source is the generator voltage, $V_g$, that appears at $z = 0$. Matrix equation (17) or (18) relates the voltages on a given transmission line segment to one another other. The voltages at the junctions are related by the junction $S$-parameters as in

$$\begin{bmatrix} V_{1,S}^{ref} \\ V_{1,1}^{ref} \\ V_{2,1}^{ref} \\ V_{2,2}^{ref} \\ V_{3,2}^{ref} \\ V_{3,L}^{ref} \end{bmatrix} = \begin{bmatrix} \rho_s & 0 & 0 & 0 & 0 & 0 \\ 0 & S_{11}^1 & S_{12}^1 & 0 & 0 & 0 \\ 0 & S_{21}^1 & S_{22}^1 & 0 & 0 & 0 \\ 0 & 0 & 0 & S_{11}^2 & S_{12}^2 & 0 \\ 0 & 0 & 0 & S_{21}^2 & S_{22}^2 & 0 \\ 0 & 0 & 0 & 0 & 0 & \rho_L \end{bmatrix} \begin{bmatrix} V_{1,S}^{inc} \\ V_{1,1}^{inc} \\ V_{2,1}^{inc} \\ V_{2,2}^{inc} \\ V_{3,2}^{inc} \\ V_{3,L}^{inc} \end{bmatrix}, \tag{19}$$

or

$$\left[V^{ref}\right] = [S] \cdot \left[V^{inc}\right] \tag{20}$$

with

$$[S] = \begin{bmatrix} \rho_s & 0 & 0 & 0 & 0 & 0 \\ 0 & S_{11}^1 & S_{12}^1 & 0 & 0 & 0 \\ 0 & S_{21}^1 & S_{22}^1 & 0 & 0 & 0 \\ 0 & 0 & 0 & S_{11}^2 & S_{12}^2 & 0 \\ 0 & 0 & 0 & S_{21}^2 & S_{22}^2 & 0 \\ 0 & 0 & 0 & 0 & 0 & \rho_L \end{bmatrix}, \tag{21}$$

where $S_{mn}^{\beta}$ is the given $S$-parameter at junction $\beta$ and $\rho_s/\rho_L$ is the reflection coefficient at the source/load. The total voltages at a junction are defined by the sum of the incident and reflected voltage waves there:

$$[V] = \begin{bmatrix} V_{1,S} \\ V_{1,1} \\ V_{2,1} \\ V_{2,2} \\ V_{3,2} \\ V_{3,L} \end{bmatrix} = \begin{bmatrix} V_{1,S}^{inc} \\ V_{1,1}^{inc} \\ V_{2,1}^{inc} \\ V_{2,2}^{inc} \\ V_{3,2}^{inc} \\ V_{3,L}^{inc} \end{bmatrix} + \begin{bmatrix} V_{1,S}^{ref} \\ V_{1,1}^{ref} \\ V_{2,1}^{ref} \\ V_{2,2}^{ref} \\ V_{3,2}^{ref} \\ V_{3,L}^{ref} \end{bmatrix}. \tag{22}$$

From (18) and (20) the incident voltages are found to be

$$\left[V^{inc}\right] = [[P] - [S]]^{-1} [V_s], \tag{23}$$

and then (22) and (18) are employed to obtain

$$[V] = [[I] + [S]] \left[V^{inc}\right], \tag{24}$$

in which $[I]$ is the identity matrix. Equation (24) relates the total junction voltages to the incident voltages, which, in view of (23) allows one to obtain the following expression for the total junction voltages

$$[V] = [[I] + [S]] [[P] - [S]]^{-1} [V_s] \tag{25}$$

in terms of the network parameters and the known column vector $[V_s]$. BLT analysis always results in an expression for the junction voltages in the form of (25).

## 3. VALIDATION

Figure 4 shows section views of the cavity configurations chosen in the data comparison. The cavity walls are assumed to perfect electric conductors and the cavities are filled with material having the properties of free space. To facilitate measurements [13, 2], parameters are selected so that the higher order modes in the *first* and *last* sections of each cavity are 'cutoff' and therefore decay rapidly as a function of displacement from apertures, loads, and sources. Photographs of the measurement apparatus are found in Figure 5. Cavity shells are

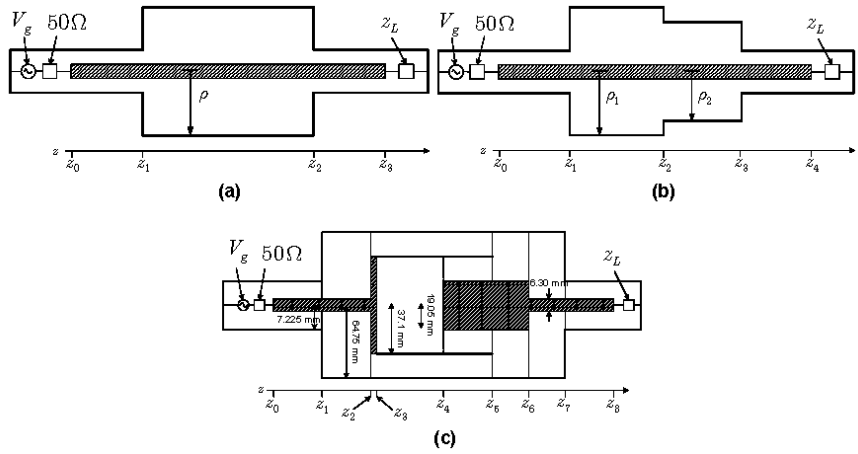


**Figure 4.** Section view of a (a) two aperture cavity, a (b) three aperture cavity, and a (c) multi-partitioned cavity with dimensions labeled.

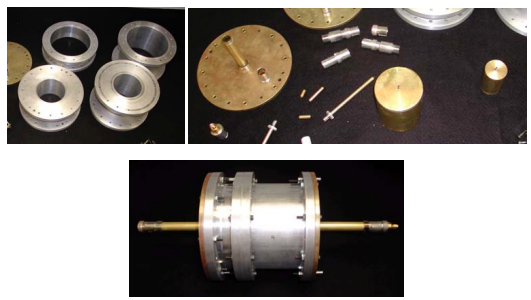

**Figure 5.** Cavity shells, cavity center conductors and loads, and external side view of the measurement apparatus.

assembled in different arrangements to construct the different cavity configurations. An input TEM wave is applied at $z = z_0$ (Figure 4), and the voltage at the first cavity aperture ($z = z_1$) and that at the load are calculated.

Figures 6–9 display results obtained from the integral equation solution method and from the transmission line method. The real part of the total voltage observed at the first aperture/junction and at the load for three different transmission line models are given in Figures 6 and 7. The TEM-only-model incorporates only one transmission line to model the wave propagation in the middle cavity section identified by $z_1 < z < z_2$ and $z_1 < z < z_3$, respectively, in Figures 4a and 4b. The additional models include additional transmission line s to model the 1st higher and 2nd higher order modes in the middle cavity section as denoted in the Figures 6 and 7. Figures 7 and 8 and display calculated results for a more complex cavity with coplanar apertures at $z = z_5$ as shown in Figure 4c. An appropriate number of modes are incorporated in each section to obtain an accurate solution over the chosen frequency range. For time domain measurements, an input pulse (Figure 10) of 0.415 V with a rise time of 50 ps or 100 ps where indicated in the figure caption and an on-time of 40 ns is applied by the generator (of 50 Ohm output impedance) to the input section of the cavity. The chosen 40 ns on-time is sufficiently long that the transients decay to zero before the pulse turns off, allowing one to interpret the data as that resulting from a step function stimulus as is typical for TDR data. In Figure 11–15, one finds the time domain responses of cavities due to a step input. The time domain responses are calculated by applying the FFT to frequency domain data. They are compared

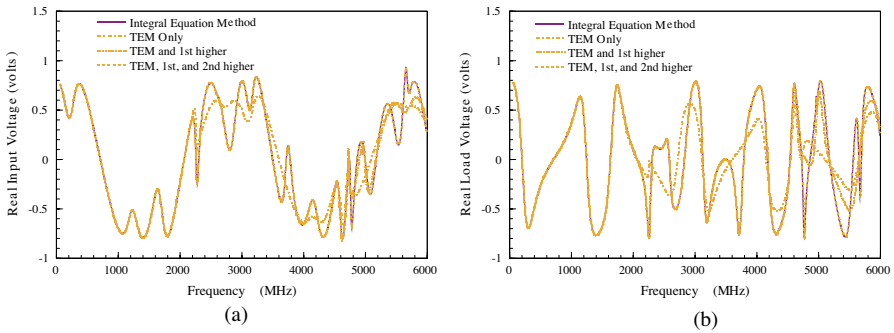


**Figure 6.** Real voltage observed at the (a) input ($z = z_1$) and the (b) load ($z = z_3$) for Cavity of Fig. 4a with $z_1 = 200\,\Omega$ ($z_1 = 0.1021$, $z_2 = 0.20378$, $z_3 = 0.30588$, $\rho = 0.06475$).

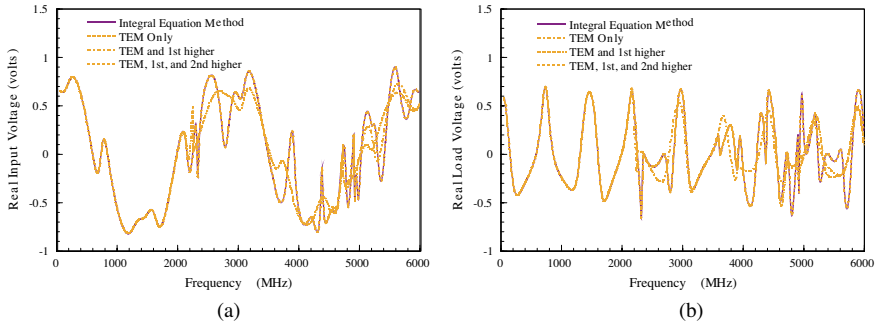


**Figure 7.** Real voltage observed at the (a) input ($z = z_1$) and the (b) load ($z = z_4$) for Cavity of Fig. 4b with $z_L = 100\,\Omega$ ($z_1 = 0.1021$, $z_2 = 0.20378$, $z_3 = 0.30588$, $z_4 = 0.40588$, $\rho_1 = 0.06475$, $\rho_2 = 0.03943$).

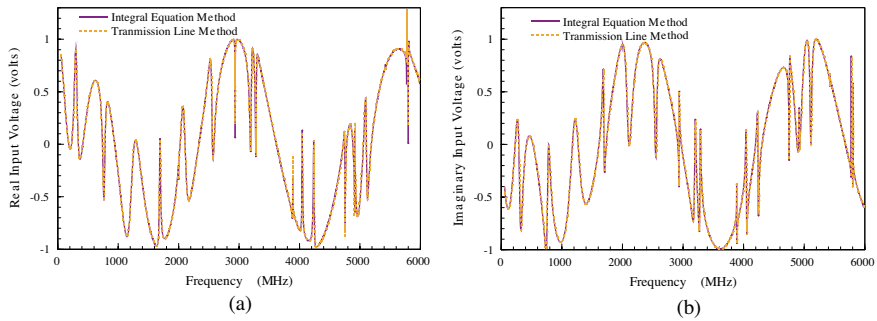


**Figure 8.** Input voltage observed at $z = z_1$ for Cavity of Fig. 4c with $z_L = \mathit{short}$ ($z_1 = 0.1021$, $z_2 = 0.12052$, $z_3 = 0.12689$, $z_4 = 0.16205$, $z_5 = 0.21404$, $z_6 = 0.22216$, $z_7 = 0.25553$, $z_8 = 0.37970$).

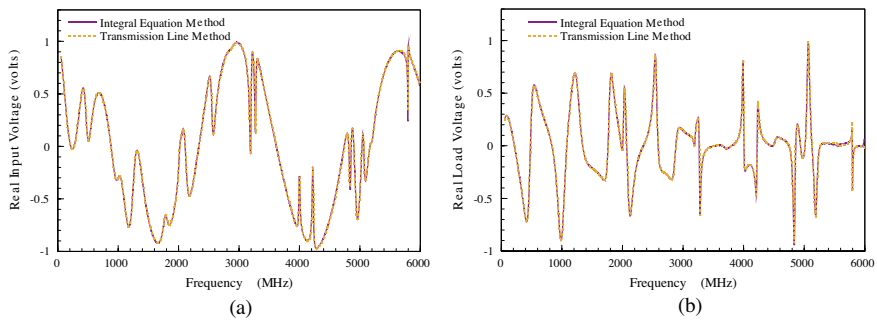


**Figure 9.** Real voltage observed at the (a) input ($z = z_1$) and the (b) load ($z = z_8$) for Cavity of Fig. 4c with $z_L = 200\,\Omega$ ($z_1 = 0.1021$, $z_2 = 0.12052$, $z_3 = 0.12689$, $z_4 = 0.16205$, $z_5 = 0.21404$, $z_6 = 0.22216$, $z_7 = 0.25553$, $z_8 = 0.41770$).

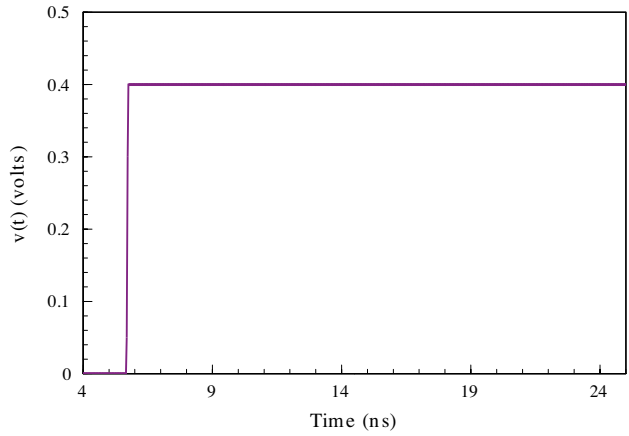


**Figure 10.** Input voltage waveform ($z = z_0$) for Figs. 11–15.

with measured values. The TDR pulse shown in Figure 10 and the measured data in Figures 11–15 are shifted in time so that the time at which the input wave reaches the cavity input ($z = z_0$) and returns to the TDR is aligned with the corresponding time for the calculated data. It is also important to note that in Figures 11–15, the 50 Ohm cable connecting the TDR to the cavity acts as a voltage divider until the propagating waveform reaches the cavity and returns, thereby resulting in an early time voltage step that appears in the measured data that does not appear in the calculated data. More details of the time domain calculations and measurements are given in [2].

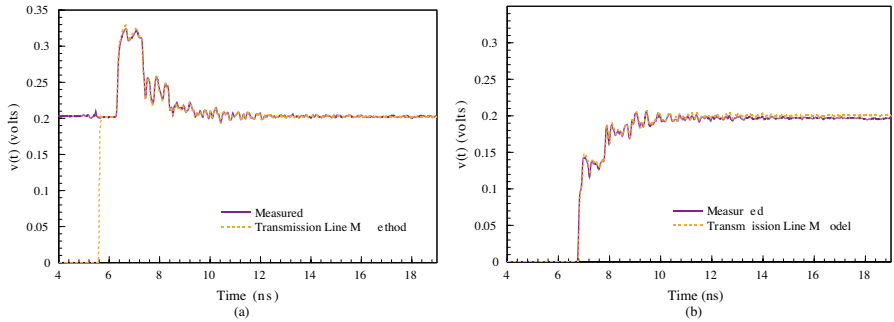


**Figure 11.** Voltage observed at the (a) generator ($z = z_0$) and the (b) load ($z = z_3$) due to a step with 50 ps rise time for Cavity of Fig. 4a with $z_L = 50\,\Omega$ ($z_1 = 0.1021$, $z_2 = 0.2555$, $z_3 = 0.3576$, $\rho = 0.06475$).

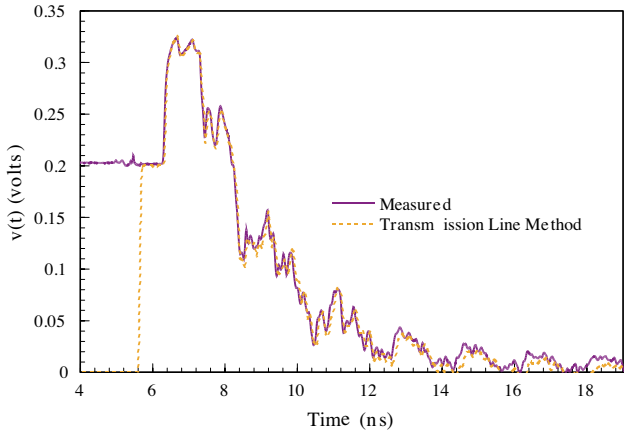


**Figure 12.** Voltage observed at the generator ($z = z_0$) due to a step with 50 ps rise time for Cavity of Fig. 4a with $z_L = short$ ($z_1 = 0.1021$, $z_2 = 0.2555$, $z_3 = 0.3816$, $\rho = 0.06475$).

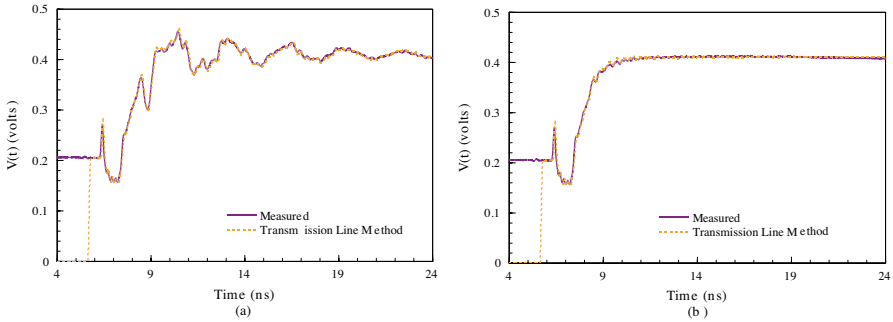


**Figure 13.** Voltage observed at the generator ($z = z_0$) for a (a) short load with $z_8 = 0.3797$ and (b) 50 Ω load due to a step with 100 ps rise time with $z_8 = 0.3877$ for cavity of Fig. 4c ($z_1 = 0.1021$, $z_2 = 0.12052$, $z_3 = 0.12689$, $z_4 = 0.18197$, $z_5 = 0.21404$, $z_6 = 0.24208$, $z_7 = 0.25530$).

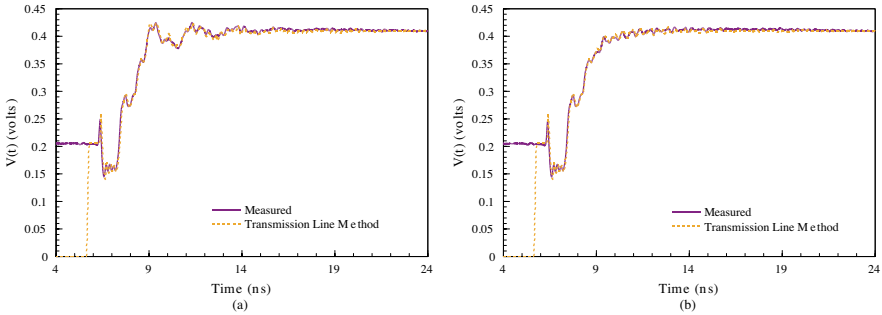


**Figure 14.** Voltage observed at the generator ($z = z_0$) for a (a) 200 Ω with $z_8 = 0.4097$ and (b) 50 Ω load due to a step with 100 ps rise time with $z_8 = 0.3877$ for cavity of Fig. 4c ($z_1 = 0.1021$, $z_2 = 0.11532$, $z_3 = 0.12169$, $z_4 = 0.16205$,$z_5 = 0.20884$, $z_6 = 0.22216$, $z_7 = 0.25530$).

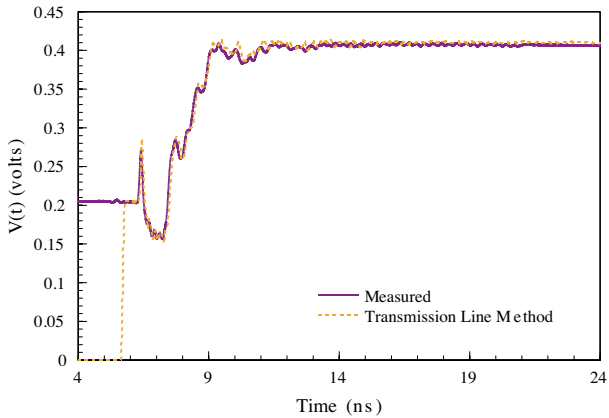


**Figure 15.** Voltage observed at the generator ($z = z_0$) for a 100 Ω load due to a step with 100 ps rise time for cavity of Fig. 4c ($z_1 = 0.1021$, $z_2 = 0.12050$, $z_3 = 0.12687$, $z_4 = 0.16205$,$z_5 = 0.21404$, $z_6 = 0.22216$, $z_7 = 0.25530$, $z_8 = 0.4097$).

## 4. CONCLUSIONS

An efficient transmission line method for finding fields in cavities containing multiple cascaded and overlapping coaxial and circular cylindrical sections is presented. Cavity sections are represented by equivalent transmission lines where each significant mode in a given section is modeled by a transmission line. Apertures joining two or more cavity sections are represented by transmission line junctions. The interactions of the cavity modes at a junction are represented by a scattering matrix. Junction voltages and currents on equivalent transmission line networks are determined efficiently by the BLT method. A carefully assembled equivalent transmission line model is shown to yield very accurate results. Input and load voltages computed with the equivalent transmission line model compare very well with values computed from the coupled integral equation technique whose accuracy is known. The cavity time domain responses computed by the equivalent transmission line model method also compare very well with measured values. Results in both the frequency and time domains are presented.

The method presented here is very efficient compared with other known techniques. A library of $S$-parameter matrices can be constructed for potential cavity junctions. Armed with this library, one can solve a wide range of cavity problems with minimal computational time. With the $S$-parameter matrices available for all junctions, the data in Figure 6 were computed in less than a second on a personal computer.

## APPENDIX A.

$S$-parameter matrix elements are calculated from the solution of an integral equation developed by Young, Butler, and Bopp [13] and extended by Bopp and Butler [2]. The equations relate the field in each cavity section to the electric field at the planar boundaries of the section. For a simple one-junction cavity (Figure 1a), we let the cavity extend to infinity in both directions. The field incident upon the junction comprises only the mode of interest for calculating the $S$-parameters parameters. The transverse field components in the cavity section defined by $z < z_2$ in Figure 1a, which we refer to as region '$a$', are of the form

$$E_{\rho,a}(\rho, z) = E^{inc}_{\rho,a} + \sum_{n=0}^{\infty} B^{-}_{a,n} e^{j\alpha_{a,n} z} \frac{d}{d\rho} \Phi_{a,n}(\rho) \tag{A1}$$

for the electric field and

$$H_{\phi,a}(\rho,z) = H_{\phi,a}^{inc} - \frac{k_a}{\eta_a}\sum_{n=0}^{\infty}\frac{1}{\alpha_{a,n}}B_{a,n}^{-}e^{j\alpha_{a,n}z}\frac{d}{d\rho}\Phi_{a,n}(\rho) \tag{A2}$$

for the magnetic field. The field components in the cavity section $z_2 < z$ in Figure 1a, which we refer to as region '$b$' are of the form

$$E_{\rho,b}(\rho,z) = \sum_{n=0}^{\infty}B_{b,n}^{+}e^{-j\alpha_{a,n}z}\frac{d}{d\rho}\Phi_{b,n}(\rho) \tag{A3}$$

and

$$H_{\phi,b}(\rho,z) = \frac{k_b}{\eta_b}\sum_{n=0}^{\infty}\frac{1}{\alpha_{b,n}}B_{b,n}^{+}e^{-j\alpha_{b,n}z}\frac{d}{d\rho}\Phi_{b,n}(\rho). \tag{A4}$$

The definitions for $k_\nu$, $\eta_\nu$, and $\alpha_{\nu,n}$ are $k_\nu = \omega\sqrt{\varepsilon_\nu\mu_\nu}$, $\eta_\nu = \sqrt{\frac{\mu_\nu}{\varepsilon_\nu}}$ and $\alpha_{\nu,n} = \sqrt{k_\nu^2 - \gamma_{\nu,n}^2}$ with subscript $\nu$ denoting a particular region with inner radius a $a_\nu$ and outer radius $b_\nu$. The $B_{\nu,n}^{\pm}$ are coefficients of the individual cavity modes and are computed from the aperture electric field. The eigenfunctions are given by

$$\Phi_{\nu,n}(\rho) = \begin{cases} N_0\left(\gamma_{\nu,n}a_\nu\right)J_0\left(\gamma_{\nu,n}\rho\right) - J_0\left(\gamma_{\nu,n}a_\nu\right)N_0\left(\gamma_{\nu,n}\rho\right), & \\ & \nu = \text{coaxial region} \\ J_0\left(\gamma_{\nu,n}\rho\right), & \nu = \text{circular cyl. region} \end{cases} \tag{A5}$$

for $n = 1, 2, 3, \ldots$. and by

$$\Phi_{\nu,0}(\rho) = \begin{cases} \ln\rho, & \nu = \text{coaxial region} \\ 1, & \nu = \text{circular cylindrical region} \end{cases} \tag{A6}$$

for $n = 0$. The eigenvalue $\gamma_{\nu,n}$ is the $n$th solution of $\Phi_{\nu,n}(b_\nu) = 0$ in region $\nu$.

In each cavity section, the only wave component traveling into the junction is the incident mode of interest. For a incident wave of mode '$m$' where $E_{\rho,a}^{inc} = E_m^{inc}e^{-j\alpha_{a,m}z}\frac{d}{d\rho}\Phi_{a,m}(\rho)$ and from (A1)–(A4), we obtain the integral equation

$$\frac{k_a}{\eta_a}\sum_{n=0}^{\infty}\frac{1}{\alpha_{a,n}}\frac{d}{d\rho}\Phi_{a,n}(\rho)\frac{1}{\left(M_{a,n}\right)^2}\int_g^h E^A(\rho,z)\rho\frac{d}{d\rho}\Phi_{a,n}(\rho)d\rho$$

$$+\frac{k_b}{\eta_b}\sum_{n=0}^{\infty}\frac{1}{\alpha_{b,n}}\frac{d}{d\rho}\Phi_{b,n}(\rho)\frac{1}{\left(M_{b,n}\right)^2}\int_g^h E^A(\rho,z)\rho\frac{d}{d\rho}\Phi_{b,n}(\rho)d\rho$$

$$= \frac{k_b}{\eta_b}\frac{2}{\alpha_{a,m}}E_m^{inc}e^{-j\alpha_{a,m}z}\frac{d}{d\rho}\Phi_{a,m}(\rho) \tag{A7}$$

where

$$(M_{\nu,n})^2 = \begin{cases} \ln\left(\dfrac{b_\nu}{a_\nu}\right), & n=0 \\ \dfrac{(b_\nu\gamma_{\nu,n})^2}{2}\left[N_0\left(\gamma_{\nu,n}a_\nu\right)J_1\left(\gamma_{\nu,n}b_\nu\right)\right. & \\ \left.-J_0\left(\gamma_{\nu,n}a_\nu\right)N_1\left(\gamma_{\nu,n}b_\nu\right)\right]^2 - \dfrac{2}{\pi^2}, & n=1,2,\cdots \end{cases} \tag{A8}$$

for a coaxial section and

$$(M_{\nu,n})^2 = \frac{(b_\nu\gamma_{\nu,n})^2}{2}J_1\left(\gamma_{\nu,n}b_\nu\right)^2, \qquad n=1,2,3\cdots \tag{A9}$$

for a circular cylindrical section. $g$ and $h$, are the inner and outer radii of the aperture located at $z_2$. With the knowledge of the aperture electric field $E^A$ found by solving (A7), we are able to compute the values of the coefficients $B^{\pm}_{\nu,n}$ and then calculate the field anywhere in the cavity.

The $S$-parameters for a given junction are determined from knowledge of the coefficients. We define $e_{n\rho}$ in (3) as

$$e^{\nu}_{n\rho} = \frac{d}{d\rho}\Phi_{\nu,n}(\rho) \tag{A10}$$

and $h_{n\phi}$ as

$$h^{\nu}_{n\phi} = \frac{k_\nu}{\eta_\nu}\frac{1}{\alpha_{\nu,n}}\frac{d}{d\rho}\Phi_{\nu,n}(\rho). \tag{A11}$$

The $S$-parameters are then defined as

$$S_{n,\nu;m,a} = \frac{B^{\pm}_{\nu,n}e^{\mp j\alpha_{\nu,n}z}}{E^{inc}_m e^{-j\alpha_{a,m}z}}, \tag{A12}$$

where '$m$' is the incident mode in region '$a$' and '$n$' is the reflected/transmitted mode in region '$\nu$.'

## REFERENCES

1. Baum, C. E., T. K. Liu, and F. M. Tesche, "On the analysis of general multiconductor transmission line networks," Interaction Note 350, Kirtland AFB, NM, 1978.

2. Bopp, III, L. Charles, and C. M. Butler, "Field in a complex cylindrical/coaxial cavity subject to time-harmonic and transient excitation," accepted by *Radio Science*, August 2004.
3. Collin, R. E., *Field Theory of Guided Waves,* McGraw-Hill, New York, 1960.
4. Hall, R. C., R. Mittra, and K. M. Mitzner. "Analysis of multilayered periodic structures using generalized scattering matrix theory," *IEEE Trans. on Antennas Prop.,* Vol. 36, 511–517, April 1988.
5. Haskal, H., "Matrix description of waveguide discontinuities in the presence of evanescent modes," *IEEE Trans. Microwave Theory Tech.,* 184–188, March 1964.
6. Kahn, W. K. and H. Kurss, "Minimum scattering antennas," *IEEE Trans. on Antennas Prop.,* 671–675, Sept. 1965.
7. Kerns, D. M., "Basis of application of network equations to waveguide problems," *J. Res. NBS,* 515–540, May 1949.
8. Kerns, D. M., *Plane-Wave Scattering-Matrix Theory of Antennas and Antenna-Antenna Interactions,* U.S. Government Printing Office, Washington, DC, 1981.
9. Lee, W., G. Zarrillo, and C. L. Law, "Simple formulas for transmission through periodic metal grids or plates," *IEEE Trans. on Antennas Prop.,* Vol. 33, 1009–1011, Sept. 1985.
10. Ling, H., "RCS of waveguide cavities: a hybrid boundary-integral/modal approach," *IEEE Trans. on Antennas Prop.,* Vol. 38, 1413–1420, Sept. 1990.
11. Mittra, R. and S. W. Lee, *Analytical Techniques in the Theory of Guided Waves,* Macmillan, New York, 1971.
12. Montgomery, C. G., *Principles of Microwave Circuits,* Office of Scientific Research and Development, NDRC, McGraw-Hill Book Co., New York, 1948.
13. Young, J. C., C. M. Butler, and C. L. Bopp, III, "Transient signals in coupled coaxial and cylindrical cavities," *Digest of 2002 USNC/URSI National Radio Science Meeting, 2002 APS/URSI Symposium,* 166, San Antonio, TX, June 2002.